This will provide a lower bound for the problem. We then can solve the ARE with $\bar{q} \gg \max(q, b)$. This artificial weight is devised based on the asymptotic properties of the problem. The critical value of the ARE problem provides an estimate for the upper value of γ_{cr}. Having obtained lower and upper estimates one should search in the relevant segment and solve the DRE [Eq. (13)] with varying γ until a finite escape time occurs within the game duration.

IV. Simulation Results

In this section, a numerical example that illustrates the merits of the trajectory-shaping-based guidance law is presented. We analyze the effect on the miss distance against a bang–bang acceleration target maneuver, which was found to be the optimal evasive maneuver under certain optimal-control and differential-game problems (e.g., Refs. 2, 6, and 7). We have assumed the same values as used in the previous example (i.e., $t_f = 4$ s, $T = 0.25$ s); hence the results of Fig. 2 apply. The lateral acceleration of the pursuer is limited to $15g$. The lateral acceleration of the target is limited to $7.5g$, giving the maneuverability ratio $\mu = 2$ (a realistic value in present-day combat scenarios). The switching point of the evasive maneuver varies in different simulation runs from the initial time to the point of closest approach of the end game. We set $b = 1000$ and consider various values for the nonnegative design parameter q. Because it is not advisable to work at (or very close to) the true conjugate value of Fig. 2, we use $\gamma = \gamma_{cr} + 0.1$.

Figure 3 depicts the miss distance as a function of the trajectory-shaping weight. As q increases, smaller miss distances are obtained, up to a certain value of q for which the miss distance approaches a minimal value almost independent of the switch point in the major (initial) part of the end game. Larger miss distances are obtained only for a limited interval of switch points $t_{go} = T$–$3T$.

Figure 4 compares the miss distances of the linear–quadratic game (LQDG) with the bounded-control game (DGL) of Ref. 2. The pursuer control in DGL is obtained by using the discontinuous control function[2]

$$u = u_{max}\,\mathrm{sign}[Z(t_{go})], \qquad t_{go} = t_f - t \tag{18}$$

where Z is the zero-effort miss distance obtained by

$$Z = x_1 + x_2 t_{go} - T^2 x_3[e^{-\theta} + \theta - 1], \qquad \theta = t_{go}/T \tag{19}$$

For most cases the results of LQDG are slightly better. Only for evasive maneuvers that take place in the time frame $t_{go} = T$–$3T$ is the performance of the bounded-control game solution superior. Assuming a uniformly distributed t_{switch}, between 0 and 4 s, we get average miss distances of 1.4 and 1.6 m for LQDG and DGL, respectively. A heuristic explanation for the contribution of the trajectory-shaping term is as follows. The classical linear–quadratic game[1] avoids maneuvering at early stages because the integral of the control term is negatively affected and deferring the maneuver is profitable. It trades off early control effort for terminal miss. Adding the new term forces the missile to react earlier to evasive maneuvers at the expense of a larger control effort, in order to remain closer to the collision course. This in fact is the underlying philosophy of the hard-bound differential-game approach that counteracts the instantaneous zero-effort miss.

V. Conclusions

The disturbance-attenuation effect of the trajectory-shaping term in linear–quadratic differential games was presented and analyzed. The solution involves a search over the possible solution domain of the associated differential Riccati equation. A contribution of this Note is to employ available results to limit the domain of search, thus simplifying the computation.

However, the main contribution of this research is in showing that by increasing the weights on the trajectory-shaping term we reduce the miss distances. The effect becomes saturated at a certain limit value. The results obtained by applying this limit are compared with the miss distances achieved by the solution of the hard-bound differential game, which leads to a highly discontinuous control. Under the present formulation we obtain similar results with a smooth controller.

Although the hard-bound differential game strategy is superior in worst-case scenarios (where sophisticated and smart targets can execute precisely timed evasive maneuvers), against randomly maneuvering targets the new guidance law has similar performance in terms of average miss distances.

In summary, to improve the performance of the classical linear–quadratic game solution against stressing target maneuvers this preliminary study advocates using for guidance law synthesis the linear–quadratic game formulation with the inclusion of a trajectory-shaping term in the cost function.

References

[1]Ben-Asher, J. Z., and Yaesh, I., *Advances in Missile Guidance Theory*, Vol. 180, Progress in Astronautics and Aeronautics, AIAA, Reston, VA, 1998, pp. 89–99.

[2]Gutman, S., "On Optimal Guidance for Homing Missiles," *Journal of Guidance and Control*, Vol. 2, No. 4, 1979, pp. 296–300.

[3]Turetsky, V., "Upper Bounds of Missile Control Based on Linear–Quadratic Differential Game," *43rd Israel Annual Conference on Aerospace Sciences* [CD-ROM], Faculty of Aerospace Engineering, Technion—Israel Inst. of Technology, Haifa, Israel, 2003.

[4]Levinson, S., Weiss, H., and Ben-Asher, J. Z., "Trajectory Shaping and Terminal Guidance Using LQ Differential Games," AIAA Paper 2002-4839, 2002.

[5]Basar, T., and Bernhard, P., *H^∞-Optimal Control and Related Minimax Design Problems*, 2nd ed. Birkhäuser, Boston, 1995, pp. 140–142.

[6]Shinar, J., and Steinberg, D., "Analysis of Optimal Evasive Maneuvers Based on a Linearized Two-Dimensional Kinematic Model," *Journal of Aircraft*, Vol. 14, No. 8, 1977, pp. 795–802.

[7]Ben Asher, J. Z., and Cliff, E. M., "Optimal Evasion Against a Proportionally Guided Pursuer," *Journal of Guidance, Control, and Dynamics*, Vol. 12, No. 4, 1989, pp. 598–600.

Earth Escape by Ideal Sail and Solar-Photon Thrustor Spacecraft

Giovanni Mengali* and Alessandro A. Quarta†
University of Pisa, I-56122 Pisa, Italy

Introduction

SOLAR sails use the solar radiation pressure on a large reflecting surface to obtain low-thrust propulsion. This technology has been identified as enabling many recent space mission concepts. An interesting application involves the study of escape trajectories from the Earth. Early contributions to this subject date back to Sands[1] and Fimple,[2] who considered initial circular orbits and used other simplifying assumptions, and to Sackett and Edelbaum.[3] Locally optimal steering laws for a flat sail have been considered in various forms by different authors.[4–6] In a recent paper Coverstone and Prussing[7] investigated the problem of Earth escape from a geosynchronous transfer orbit with an ideal flat sail through a sail-force control algorithm that maximizes the instantaneous rate of increase of the total orbital energy. In their analysis a spherical gravity model for the Earth is assumed, and only the solar gravitational perturbation is included.

Received 4 May 2004; revision received 6 July 2004; accepted for publication 23 July 2004.

*Associate Professor, Department of Aerospace Engineering; g.mengali@ing.unipi.it.

†Ph.D. Candidate, Department of Aerospace Engineering; a.quarta@ing.unipi.it.

The conventional ideal flat sail is known to be quite inefficient at high values of the sail cone angle α due to the fact that the thrust exerted by the solar radiation pressure is proportional to $\cos^2\alpha$. Significant performance improvements over a flat sail may be obtained by separating the functions of collecting and directing the solar radiation, as is done by a solar photon thrustor (SPT).[8,9] In fact, the thrust for a SPT sail is proportional to $\cos\alpha$. Despite this, a detailed engineering study of an SPT sail has not yet been performed.

This Note extends the results by Coverstone and Prussing[7] in various ways. First, assuming the same control logic aimed at maximizing the instantaneous rate of energy change, a compact expression for the control law of a SPT sail is derived using vector notation. Second, a comparison is made with the performance of a flat ideal solar sail. Third, in addition to the solar gravitational attraction, other perturbations on the solar-sail trajectory are taken into account. These include the Earth oblateness, the lunar gravitational attraction, the shadowing effects of the Earth, and the variation in the magnitude of the solar flux due to the eccentricity of the Earth's orbit.

Equations of Motion

The equations of motion for a solar sail with respect to a geocentric inertial frame $\mathcal{T}_\oplus(x, y, z)$ are

$$\dot{\boldsymbol{r}} = \boldsymbol{v} \tag{1}$$

$$\dot{\boldsymbol{v}} = -\left(\mu_\oplus / r^3\right)\boldsymbol{r} + \boldsymbol{a}_p + \boldsymbol{a} \tag{2}$$

where $[\boldsymbol{r}]_{\mathcal{T}_\oplus} = [r_x, r_y, r_z]^T$ and $[\boldsymbol{v}]_{\mathcal{T}_\oplus} = [v_x, v_y, v_z]^T$ are the position and velocity vectors of the spacecraft relative to $\mathcal{T}_\oplus$, $r \triangleq \|\boldsymbol{r}\|$ is the spacecraft distance from the Earth, $\boldsymbol{a}_p$ is the total disturbing acceleration, $\boldsymbol{a}$ is the acceleration due to the solar radiation pressure, and $\mu_\oplus$ is the Earth's gravitational parameter. In this Note both the perturbations due to the lunisolar gravitational attraction[10] and the Earth oblateness effects[11] (up to J_6) are taken into account. Assuming that the solar sail is a flat, perfectly reflecting body, the propelling acceleration $\boldsymbol{a}$ exerted by the solar radiation pressure P is given by

$$\boldsymbol{a} = (2PA\eta/m)(\hat{\boldsymbol{r}}_{\odot s} \cdot \hat{\boldsymbol{a}})^p \hat{\boldsymbol{a}} \tag{3}$$

where A is the sail area, m is the spacecraft mass, $\hat{\boldsymbol{r}}_{\odot s} \triangleq (\boldsymbol{r} - \boldsymbol{r}_\odot)/\|\boldsymbol{r} - \boldsymbol{r}_\odot\|$ is the unit vector in the direction of the incident radiation from the sun, and $\hat{\boldsymbol{a}} \triangleq \boldsymbol{a}/a$ is the unit vector in the direction of thrust (Fig. 1). The index p is used to define the type of solar sail, with $p = 2$ corresponding to a flat solar sail and $p = 1$ corresponding to a SPT spacecraft. Also, the term $\eta \in [0, 1]$ represents the shadow function,[12] which establishes the spacecraft umbra ($\eta = 0$) and penumbra ($0 < \eta < 1$) conditions. Of course, $\eta = 1$ corresponds to a solar sail that is outside the shadow envelope. The geocentric ephemeris for the sun ($\boldsymbol{r}_\odot$) and the Moon are based on the Jet Propulsion Laboratory DE200/LE200 model.[13,14] This allows one to take into account the time variation in the magnitude of the solar flux (about 6% in 1 year) due to the Earth's orbit eccentricity. Note that $\hat{\boldsymbol{a}}$ is normal to the sail as long as an ideal flat-sail model is assumed.

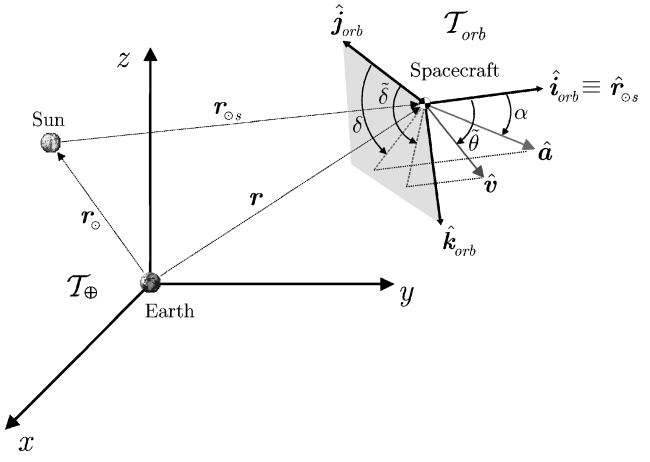

Fig. 1 Reference frames and main geometric parameters.

Under the hypothesis that the solar radiation pressure has an inverse-square variation with the distance $r_{\odot s}$ from the sun, one has

$$\frac{PA}{m} = \frac{\beta}{2}\frac{\mu_\odot}{r_{\odot s}^2} = \frac{a_c \sigma^* \mu_\odot}{4 P_\oplus r_{\odot s}^2} \tag{4}$$

where m is the spacecraft mass, $\beta \triangleq \sigma^*/\sigma$ is the solar-sail lightness number, that is, the ratio between the critical solar-sail loading parameter $\sigma^* \triangleq 1.539$ g/m^2 and the sail loading $\sigma \triangleq m/A$ (see Ref. 9, p. 40), a_c is the characteristic acceleration of the solar sail, and $P_\oplus \cong 4.557 \times 10^{-6}$ N/m^2 is the solar radiation pressure at 1 AU.

Let $\mathcal{T}_{\text{orb}}(x_{\text{orb}}, y_{\text{orb}}, z_{\text{orb}})$ be an orbital frame whose unit vectors are $\hat{\boldsymbol{i}}_{\text{orb}} \equiv \hat{\boldsymbol{r}}_{\odot s}, \hat{\boldsymbol{j}}_{\text{orb}}$ and $\hat{\boldsymbol{k}}_{\text{orb}}$. Assume that the plane $z_{\text{orb}} = 0$ contains the axis z of the $\mathcal{T}_\oplus$ frame and y_{orb} points toward the Earth's north pole. It is useful to express the components of $\hat{\boldsymbol{a}}$ in the $\mathcal{T}_{\text{orb}}$ frame as a function of the thrust cone angle $\alpha \triangleq \arccos(\hat{\boldsymbol{r}}_{\odot s} \cdot \hat{\boldsymbol{a}}) \in [0, \pi/2]$ and of the thrust clock angle $\delta \in [-\pi, \pi]$ (see Fig. 1). One has

$$[\hat{\boldsymbol{a}}]_{\mathcal{T}_{\text{orb}}} = [\cos\alpha, \sin\alpha\cos\delta, \sin\alpha\sin\delta]^T \tag{5}$$

From Eqs. (3) and (4) it is clear that, for the same $r_{\odot s}$ and β, a SPT gives a propelling acceleration $\|\boldsymbol{a}_{\text{SPT}}\|$ greater than the corresponding acceleration of a flat sail $\|\boldsymbol{a}_{\text{flat}}\|$ at angles $0 < \alpha < \pi/2$. At $\alpha = 0$ and $\alpha = \pi/2$ the accelerations are the same. The maximum difference between $\|\boldsymbol{a}_{\text{SPT}}\|$ and $\|\boldsymbol{a}_{\text{flat}}\|$ (equal to 25% of $\|\boldsymbol{a}_{\text{flat}}\|$) is obtained when $\alpha = \pi/3$.

Escape Control Law

Following Coverstone and Prussing,[7] an efficient method of increasing the total orbital energy E is to maximize the instantaneous rate of energy change. Although this control logic does not determine minimum-time escape results, it has been found[7] that the corresponding trajectories are near-minimum-time solutions as long as low sail accelerations (on the order of $10^{-4}g$) are considered. This is exactly the assumption made in this Note.

The escape control law is obtained as follows: Taking the scalar product of the equation of motion (2) with the solar sail velocity vector $\boldsymbol{v}$ and recalling that $E = \frac{1}{2}\boldsymbol{v}\cdot\boldsymbol{v} - \mu_\oplus/r$ yields

$$\dot{E} = \boldsymbol{a}_p \cdot \boldsymbol{v} + \boldsymbol{a} \cdot \boldsymbol{v} \tag{6}$$

The problem is that of finding the control law $\boldsymbol{u}(t) = [\alpha(t), \delta(t)]^T$ that at any given time, maximizes the component of the sail acceleration along the velocity vector. This amounts to maximizing the performance index $J \triangleq \boldsymbol{a} \cdot \boldsymbol{v}$, that is,

$$\boldsymbol{u} = \arg\max_{\boldsymbol{u}\in\mathcal{U}} J \tag{7}$$

where $\mathcal{U}$ is the domain of feasible controls. The components of the velocity vector $\boldsymbol{v}$ in the $\mathcal{T}_{\text{orb}}$ frame are given by

$$[\boldsymbol{v}]_{\mathcal{T}_{\text{orb}}} = v[\cos\tilde{\theta}, \sin\tilde{\theta}\cos\tilde{\delta}, \sin\tilde{\theta}\sin\tilde{\delta}]^T \qquad \text{with} \qquad \tilde{\theta} \in [0, \pi] \tag{8}$$

where $\tilde{\theta}$ and $\tilde{\delta}$ are the velocity vector cone and clock angle, respectively (see Fig. 1). Substituting Eqs. (3) and (5) into Eq. (7) one has

$$J = \left[\eta\beta\left(\mu_\odot / r_{\odot s}^2\right)v\right]\cos^p\alpha(\cos\alpha\cos\tilde{\theta} + \sin\alpha\cos\delta\sin\tilde{\theta}\cos\tilde{\delta} + \sin\alpha\sin\delta\sin\tilde{\theta}\sin\tilde{\delta}) \tag{9}$$

The control angles α and δ that maximize J are obtained by letting $\partial J/\partial\boldsymbol{u} = 0$. The result is

$$\tan\alpha = \frac{-(1+p)\cos\tilde{\theta} + \sqrt{(1+p)^2\cos^2\tilde{\theta} + 4p\sin^2\tilde{\theta}}}{2p\sin\tilde{\theta}} \qquad \text{for} \qquad \tilde{\theta} \in [0, \pi] \tag{10}$$

$$\tan\delta = \tan\tilde{\delta} \tag{11}$$

As long as a flat-sail model is assumed ($p = 2$), Eq. (10) gives the control law, which agrees with the results found in the literature.[4,7]

On the other hand, assuming a SPT model ($p = 1$), Eq. (10) reduces to the following simple relationship:

$$\alpha_{\mathrm{SPT}} = \tilde{\theta}/2 \qquad \text{for} \qquad \tilde{\theta} \in [0, \pi] \tag{12}$$

As a consequence of Eq. (11), the unit vectors $\hat{\boldsymbol{a}}$, $\hat{\boldsymbol{r}}_{\odot s}$, and $\hat{\boldsymbol{v}} \triangleq \boldsymbol{v}/v$ are coplanar. This allows one to remove the dependence on $\hat{\boldsymbol{a}}$ in the equations of motion [see Eqs. (2) and (5)]. The result is

$$\hat{\boldsymbol{a}} = \begin{cases} \dfrac{\sin(\tilde{\theta} - \alpha)}{\sin\tilde{\theta}}\hat{\boldsymbol{r}}_{\odot s} + \dfrac{\sin\alpha}{\sin\tilde{\theta}}\hat{\boldsymbol{v}} & \text{for} \quad \tilde{\theta} \in (0, \pi) \\ \hat{\boldsymbol{r}}_{\odot s} & \text{for} \quad \tilde{\theta} = 0 \end{cases} \tag{13}$$

where

$$\cos\tilde{\theta} = \hat{\boldsymbol{v}} \cdot \hat{\boldsymbol{r}}_{\odot s}, \qquad \sin\tilde{\theta} = |\hat{\boldsymbol{v}} \times \hat{\boldsymbol{r}}_{\odot s}| \tag{14}$$

Observe that $\tilde{\theta} = \pi$ corresponds to $\alpha = \pi/2$ [see Eq. (10)]. Accordingly, in this case all the terms containing $\hat{\boldsymbol{a}}$ vanish in the equations of motion (because $\boldsymbol{a} = 0$). Finally, from Eqs. (12) and (13) the acceleration unit vector for a SPT model is given by

$$\hat{\boldsymbol{a}}_{\mathrm{SPT}} = \sqrt{1/[2(1 + \cos\tilde{\theta})]}(\hat{\boldsymbol{r}}_{\odot s} + \hat{\boldsymbol{v}}) \qquad \text{for} \qquad \tilde{\theta} \in [0, \pi) \tag{15}$$

Illustrative Results

The control laws previously described have been applied to simulating escape trajectories from the Earth using an ideal flat sail and a SPT spacecraft. A set of canonical units[15] $\mathrm{DU}_{\oplus} \triangleq 6378.13655$ km and $\mathrm{TU}_{\oplus} \triangleq 806.81103$ s ($\mu_{\oplus} = 1\ \mathrm{DU}_{\oplus}^3/\mathrm{TU}_{\oplus}^2$) have been used in the integration of the equations of motion (1) and (2) to reduce their numerical sensitivity. The differential equations were integrated in double precision using a Runge–Kutta fifth-order scheme with absolute and relative errors of 10^{-12}. For comparative purposes, the initial orbit is taken to be an Ariane 5 geosynchronous transfer orbit, with an inclination angle of 7 deg with respect to the equatorial plane, an eccentricity $e = 0.716$, and a perigee altitude of 600 km.

For each of the two solar sails (flat and SPT), three different models are considered. The first (referred to as model a) neglects all the perturbative effects on the sail [i.e., $\boldsymbol{a}_p = 0$ in Eq. (2)] and the shadowing effects of the Earth [i.e., $\eta \equiv 1$ in Eq. (3)]. The second, model b, differs from model a in that it includes the shadow conditions. Finally, model c considers both the shadow conditions and the perturbative effects due to the lunisolar gravitational attraction and the Earth oblateness.

All the simulations have been performed with the same initial orbit orientation and using a characteristic acceleration[7] equal to $a_c = 0.93$ mm/s^2. In particular, it has been assumed that the longitude of the ascending node is $\Omega = 180$ deg and the argument of the periapsis is $\omega = 270$ deg. The simulations start when the true anomaly is zero. Also, recall that the geocentric ephemerides for both sun and Moon have been taken into account.

The times required to achieve escape energy for a number of different deployment dates in the range 1/1/2004–12/31/2004 are shown in Fig. 2. Simulations have been performed assuming a spacecraft deployment corresponding to the 1st and the 21st of each month. The lack of some points in the figure reveals that in some cases the perigee radius has dropped below the Earth's surface. The possibility of such a situation has been reported in the literature.[7] This problem may be alleviated with the aid of a blended controller, as suggested by Macdonald and McInnes.[4] Figure 2 clearly illustrates the superiority of a SPT spacecraft over a flat sail, with a mean reduction of escape time on the order of 15% for the three models.

The deployment date has a significant effect on the efficiency of the escape maneuver, with no apparent trend for increasing or decreasing the escape time. The link between departure date and Earth escape time has been investigated by Macdonald and McInnes.[16] Note that in some cases, model c (which includes all the perturbations) behaves better than model a. The main reason for this behavior is that the escape condition is heavily influenced by the spacecraft position with respect to the sun when the spacecraft energy is near

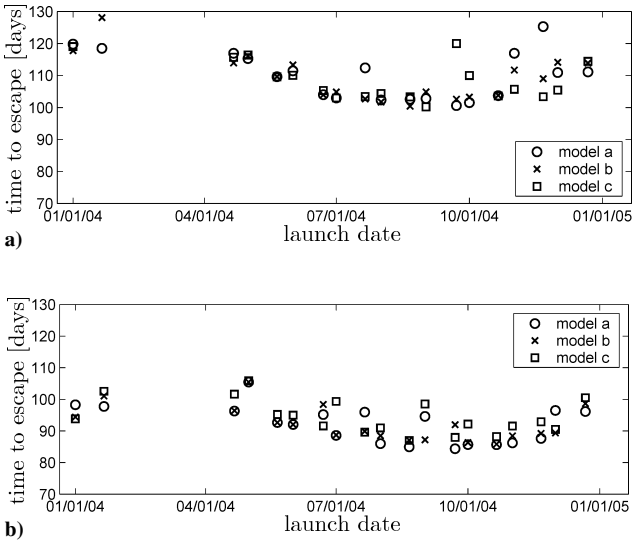

Fig. 2 Times to escape for a) a flat sail and b) a solar-photon thrustor.

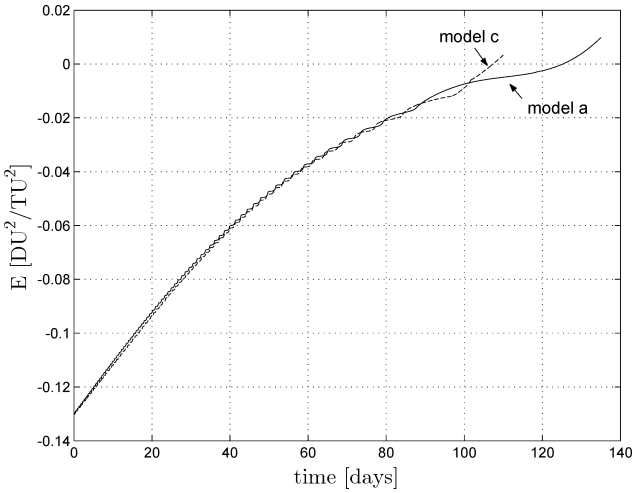

Fig. 3 Time history of energy increase for a flat sail with different perturbation models (starting date 11/21/2004).

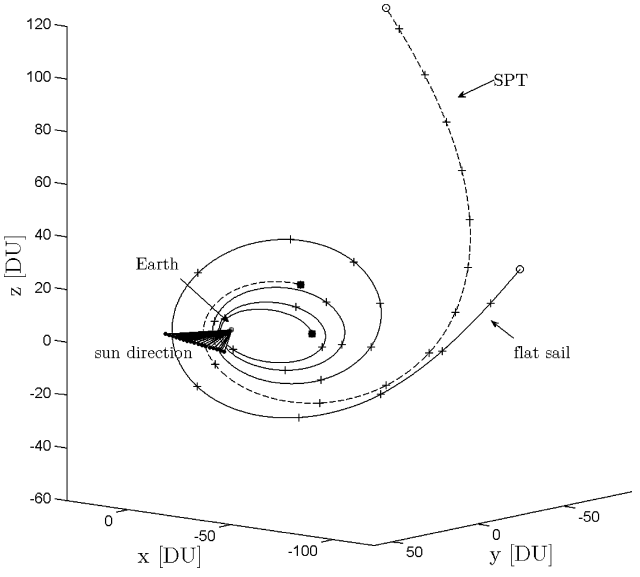

Fig. 4 Three-dimensional view of the solar-sail trajectories (starting date 11/21/2004) for a flat sail and a SPT spacecraft. The black square represents the solar-sail position after 70 days; the white circle corresponds to the escape condition. Crosses are represented with a time interval of 2 days.

(but less than) the critical value. The variation in escape time for the three different models is likely due to the different sun–sail positions in the last few spirals before the escape condition is reached. In some cases, initially similar spirals can require an extra half revolution to reach escape, resulting in a somewhat erratic profile of escape time as a function of launch date. The situation is illustrated in Fig. 3 for an ideal sail. The slope of the energy plot for model a and model c are nearly identical in the first 80 days. After that time, the spacecraft is far enough from the Earth to gain significantly different accelerations in the two cases. Assuming November 21, 2004 as a starting date and a full set of perturbative effects (model c), a comparison between the trajectories of an ideal flat sail and a SPT spacecraft is shown in Fig. 4.

Conclusions

Escape trajectories from geosynchronous transfer orbit for solar sails have been investigated. A simple control, which maximizes the instantaneous rate of energy change, has been derived using vector notation. The control law comprises both the case of an ideal flat sail and the case of a solar-photon thrustor spacecraft. The latter configuration possesses superiority over a flat sail, with a mean reduction of escape times on the order of 15%. The analysis takes into account the most important perturbative effects on the solar sail and shows the importance of such effects on the escape maneuver. The simulations clearly indicate that the sun–sail position in the last few spirals has a significant effect on the efficiency of the escape trajectory.

Acknowledgments

The authors acknowledge the useful comments of Associate Editor Colin McInnes, which helped improve the presentation of this paper.

References

[1]Sands, N., "Escape from Planetary Gravitational Fields by Use of Solar Sails," *American Rocket Society Journal*, Vol. 31, No. 4, 1961, pp. 527–531.

[2]Fimple, W. R., "Generalized Three-Dimensional Trajectory Analysis of Planetary Escape by Solar Sail," *American Rocket Society Journal*, Vol. 32, No. 6, 1962, pp. 883–887.

[3]Sackett, L. L., and Edelbaum, T. N., "Optimal Solar Sail Spiral to Escape," AAS/AIAA Astrodynamics Conf., Sept. 1977.

[4]Macdonald, M., and McInnes, C. R., "Analytic Control Laws for Near-Optimal Geocentric Solar Sail Transfers," American Astronautical Society, AAS Paper 01-472, Aug. 2001.

[5]Fekete, T. A., Sackett, L. L., and von Flotow, A. H., "Trajectory Design for Solar Sailing from Low-Earth Orbit to the Moon," *Advances in the Astronautical Sciences*, Vol. 79, Feb. 1992, pp. 1083–1094.

[6]Leipold, M., "Solar Sail Mission Design," Ph.D. Dissertation, Technische Universität München, DLR FB 2000 22, Munich, Germany, Feb. 2000.

[7]Coverstone, V. L., and Prussing, J. E., "Technique for Escape from Geosynchronous Transfer Orbit Using a Solar Sail," *Journal of Guidance, Control, and Dynamics*, Vol. 26, No. 4, 2003, pp. 628–634.

[8]Forward, R. L., "Solar Photon Thrustor," *Journal of Spacecraft and Rockets*, Vol. 27, No. 4, 1990, pp. 411–416.

[9]McInnes, C. R., *Solar Sailing: Technology, Dynamics and Mission Applications*, Springer-Verlag, Berlin, 1999, pp. 40, 91–95.

[10]Battin, R. H., *An Introduction to the Mathematics and Methods of Astrodynamics*, AIAA Education Series, AIAA, New York, 1987, pp. 387–391.

[11]Roy, A. E., *Orbital Motion*, 3rd ed., Institute of Physics Publishing, Bristol, England, U.K., pp. 511, 512.

[12]Montenbruck, O., and Gill, E., *Satellite Orbits: Models, Methods, and Applications*, Springer-Verlag, Berlin, 2000, pp. 81–83.

[13]Standish, E. M., "Orientation of the JPL Ephemerides, DE200/LE200, to the Dynamical Equinox of J2000," *Astronomy and Astrophysics*, Vol. 114, No. 2, 1982, pp. 297–302.

[14]Standish, E. M., "The Observational Basis for JPL's DE200, the Planetary Ephemeris of the Astronomical Almanac," *Astronomy and Astrophysics*, Vol. 233, No. 1, 1990, pp. 252–271.

[15]Standish, E. M., "Report of the IAU WGAS Sub-Group on Numerical Standards," Technical Rept., IAU Working Group on Astronomical Standards, URL: http://ssd.jpl.nasa.gov/iau-comm4/iausgnsrpt.ps [cited 28 Sept. 2004].

[16]Macdonald, M., and McInnes, C. R., "Seasonal Efficiencies of Solar Sailing in Planetary Orbit," 53rd International Astronautical Congress, IAC-02-S.6.01, Oct. 2002.